Climate Dynamics (2020) 55:2237–2252
https://doi.org/10.1007/s00382-020-05380-6

Climatology of Tibetan Plateau vortices derived from multiple reanalysis datasets

Zhiqiang Lin[1,2] · Weidong Guo[1,3] · La Jia[4] · Xiuping Yao[5] · Zhenbo Zhou[4]

Received: 8 December 2019 / Accepted: 13 July 2020 / Published online: 17 July 2020

Abstract

The Tibetan Plateau vortex (TPV) is a mesoscale weather system active in the near-surface layer, which is one of the major systems for the generation of precipitation in the Tibetan Plateau (TP). However, no long-term observations of the TPVs are available due to the scarcity of observations in the TP. Thereby, long-term, high-accuracy reanalysis products are a reliable source for the analysis of characteristic TPV activities and possible mechanisms behind. In the present study, an objective analysis method is implemented to obtain a complete dataset of TPV based on several reanalysis products, including the ERA-Interim, ERA40, JRA55, NCEP CFSR, and NASA MERRA2. The TPVs are detected and tracked by the minima in geopotential height at 500 hPa. Results indicate that the TPVs derived from multiple reanalysis products have quite similar spatial patterns and temporal variability. The characteristic parameters of the TPVs derived from a given reanalysis data are related to the resolution of this reanalysis product. Higher-resolution reanalysis products can yield more low-pressure systems, which explains why the TPVs derived from high-resolution reanalysis datasets generally have longer lifetime, stronger and larger vortex scale than those from low-resolution reanalysis products, although the total number of TPVs are similar. The annual average number of TPVs generated in the TP is 63.5, and these TPVs largely originate in the mountainous area of the central western TP around (34° N, 78–95° E) and a belt zone (30° N, 80–84° E) in the southern TP, where the elevation is around 5500 m. The TPVs often dissipate in low valleys and the lee side of mountains. They mainly occur in the warm season during May–September, most active in the summer and least active in the winter. More TPVs form in the daytime than in the nighttime. Those TPVs that move out of the TP account for less than 10–14% of all TPVs, and they usually follow three moving paths: eastward (6.9–7.8%), northeastward (2.3–3.4%) and southward (2.3–3.5%).

Keywords Tibetan Plateau · Tibetan Plateau Vortex · Objective analysis · Reanalysis products · Spatial–temporal characteristics

1 Introduction

The Tibetan Plateau (TP) is surrounded by the Kunlun Mountains in the north, the Himalayas in the south, the Pamir in the west, and the Hengduan Mountains in the east. The average elevation of the TP is above 4000 m, covering an area of 2.9-million km^2. It is the largest and highest plateau in the world, known as the "Third Pole" (Qiu 2008). It is the source of many major rivers in Asia, providing water for millions of people, and therefore is called the "Asian Water Tower" (Immerzeel et al. 2010; Xu et al. 2008a; Yao et al. 2012). Since the major water supply for the "Asian Water Tower" is precipitation on the TP, it is important to study the spatial pattern and temporal variability of precipitation and related weather systems.

Electronic supplementary material The online version of this article (https://doi.org/10.1007/s00382-020-05380-6) contains supplementary material, which is available to authorized users.

✉ Weidong Guo
guowd@nju.edu.cn

1 Institute for Climate and Global Change Research, School of Atmospheric Sciences, Nanjing University, Nanjing 210023, Jiangsu, China

2 Tibet Institute of Plateau Atmospheric and Environmental Science, Lhasa, China

3 Joint International Research Laboratory of Atmospheric and Earth System Sciences, Nanjing, China

4 Tibetan Meteorological Observatory, Meteorological Bureau of Tibet Autonomous Region, Lhasa, China

5 China Meteorological Administration Training Center, China Meteorological Administration, Beijing, China

The Tibetan Plateau vortex (TPV) is one of the major systems for the generation of precipitation in the TP (Ye and Gao 1979; Ye 1981; Zhang et al. 2014; Yu et al. 2014) and an important weather pattern for strong convection (Tao and Ding 1981; Hu et al. 2017; You et al. 2015). It should be mentioned that the abbreviation "TPV" is also used for "tropopause polar vortices" (e.g. Cavallo and Hakim 2013). As the upstream region of the atmospheric circulation in China, the eastward moving vortex system formed in the TP has pronounced influences in precipitation over most of China, especially the Yangtze River basin (Tao and Ding 1981; Zhang et al. 2001; Yu et al. 2014; Lin et al. 2016). The moving off TPV and the Southwest Vortex are active in the lee side of the TP, and once coupled, they can bring heavy precipitation and disastrous strong convective weather (Li et al. 2017; Yu et al. 2016). The flooding that occurred in the Yangtze River Basin in 1998, which caused huge economic losses and casualties, is closely related to the large convective cloud system induced by the eastward moving TPV (National Meteorological Center and National Satellite Meteorological Center 1998). Thereby, the study of the TPV has been highly valued in the meteorological community of China.

The TPV is a shallow weather system active in the near-surface layer of the TP, mostly identified at 500 hPa (Ye and Gao 1979). The formation and development of the TPV are highly correlated with the thermodynamic forcing of the TP and the latent heat release caused by active convection (Lhasa Research Group on Qinghai-Xizang Plateau Meteorology 1981; Wang 1987; Dell'osso and Chen 1986; Shen et al. 1986a, b; Li et al. 2014b). Due to the harsh natural environment and sparse observation network (Xu et al. 2008b), there still exist many ambiguities in the study of the TPV. For example, the occurrence frequency of the TPV is much higher in 1979 than in other years, which is probably attributed to the increased observations obtained in the Atmospheric Science Experiment in the Tibetan Plateau conducted in 1979 (Qian et al. 1984). Traditionally, the investigation of the TPV heavily relies on manual examination of weather maps. A TPV is subjectively identified if there is a closed low pressure system at 500 hPa or cyclonic circulation appears at least at three weather stations in the TP. Forecasters often have different opinions regarding whether the TPV exists even if they are examining the same weather map. This subjective method to identify the TPV leads to large uncertainties in the TPV study, and makes it hard to accurately describe the TPV climatology.

At present, high spatiotemporal resolution data like various reanalysis products have become major sources for analysis of weather systems such as the extratropical cyclones, etc. (Neu et al. 2013). A number of the TPV studies including both single cases studies and climatic studies are based on reanalysis datasets, for example the works of Li et al. (2014a, b, c), Feng et al. (2014), Lin (2015), Li et al. (2011, 2018a, b), Curio et al. (2018, 2019) and references therein. However, a dataset of the TPVs derived from multiple reanalyses is still absent so far. In particular, what are the common features of the TPVs shown in various reanalysis products that are widely used, and what are the differences between them? These questions still remain unanswered. The study based on multiple reanalysis products can help people to understand the TPV characteristics from multiple perspectives and reduce uncertainties in a given dataset.

In the present study, a TPV dataset based on several most advanced reanalysis products is obtained using an objective identification method for the purpose of the TPV climatology study. Section 2 introduces the reanalysis datasets used in the present study and the TPV identification method. The spatiotemporal variation characteristics of the TPV including its spatial pattern and seasonal and inter-annual variabilities are described in Sect. 3. Section 4 analyzes the relative frequency distributions of TPV attributes in their characteristic ranges. The moving paths of the TPV derived from various reanalysis products are compared in Sect. 5. Sections 6 and 7 presents the discussions and summary, respectively.

2 Data and method

2.1 Reanalysis datasets

Five reanalysis products: the European Centre for Medium-Range Weather Forecasts (ECMWF) Re-Analysis Interim (ERA-Interim, hereafter ERAI) (Dee et al. 2011), the 40-years ECMWF Re-Analysis (ERA40) (Uppala et al. 2005), the Japanese 55-year Reanalysis (JRA55) (Kobayashi et al. 2015), the National Centers for Environmental Prediction (NCEP) Climate Forecast System Reanalysis (CFSR) (Saha et al. 2010) and the National Aeronautics and Space Administration (NASA) Modern-Era Retrospective Analysis for Research and Applications version 2 (MERRA2) (Gelaro et al. 2017), are used in the present study. Table 1 lists brief information of all the five reanalysis products. All the data have the temporal resolution of 6-hourly, despite the fact that CFSR and MERRA2 can provide higher temporal resolution outputs via numerical models. Bao and Zhang (2013) used the 6-hourly radiosondes collected during the Tibetan Plateau Experiment (TIPEX) to evaluate the reanalysis datasets. They found that the reanalysis data can produce consistent circulations (horizontal winds in their study) with independent sounding observations that are not assimilated into the reanalysis. They also found that the newer generation reanalysis products (ERAI and CFSR) are better than their previous versions. This provides a solid basis for the TPV climatology study using reanalysis products. ERAI and CFSR are used to obtain TPVs in the studies of Feng et al.

Table 1 Details of the reanalysis datasets used in this study, including their spatial resolutions and periods

Dataset	Spatial resolution (latitude × longitude)	Period	Minimum radius/average relative vorticity should be satisfied for at least 3 time steps
ERA-Interim	1° × 1°	Jan 1979–Dec 2017	145 km/1 × 10^{-5} s^{-1}
ERA40	1° × 1°	Jan 1958–Dec 2001	140 km/1 × 10^{-5} s^{-1}
JRA55	1.25° × 1.25°	Jan 1958–Dec 2017	60 km/1 × 10^{-5} s^{-1}
CFSR	0.5° × 0.5°	Jan 1979–Dec 2017	170 km/1 × 10^{-5} s^{-1}
MERRA2	1/2° × 2/3°	Jan 1980–Dec 2017	155 km/1 × 10^{-5} s^{-1}

(2014), Lin (2015) and Curio et al. (2019), and the ERA40, JRA55 and MERRA2 are first used to produce TPVs. In the present study, we compare our results with those from the previous studies in Sect. 6.

2.2 The method to identify the TPV

The TPVs are identified and tracked based on geopotential height at 500 hPa using the scheme of Lin (2015), which is derived from the method for extratropical cyclones identification proposed by Wernli and Schwierz (2006, hereinafter referred to as WS06). Though WS06 was developed for the extratropical cyclones, it could be adopted to the identification and analyses of different kind of synoptic systems by using some specific threshold. The algorithm is applied to the domain of 40–160° E and 15–65° N. Detailed steps are described as follows.

(1) The local minimum and maximum of geopotential height at 500 hPa is identified and labeled based on comparison with that in the surrounding eight cell grids, as shown in Fig. S1a.

(2) Tracing the contours of geopotential height at 500 hPa using an interval of 1 gpm. The contours unclosed or embedded within local maximum are removed, and the closed contours with a radius of larger than 10^3 km are also removed since the horizontal size of TPVs is far smaller than that, as shown in Fig. S1b. The average position of the innermost closed contour is taken as the candidate low center, as shown in Fig. S1c.

(3) When two or more candidate lows are embedded within the same outer closed contour, three procedures will be operated: (a) if the lows are too close to each other (within 5° latitude/longitude), the weaker one (with higher geopotential height) will be removed, as shown in Fig. S2a; (b) if the adjacent lows described in condition (a) are with equal intensity, the lows and their innermost contours will be removed and a new low will be created, as shown in Fig. S2b; (c) if the lows are more than 5° latitude/longitude apart from each other, the outer closed contour will be removed and the lows are taken as single ones, as shown in Fig. S2c.

(4) All low-pressure systems are obtained using a track determination method that considers the persistence of the weather system (Wernli and Schwierz 2006). In order to exclude the heat lows, the low-pressure systems with a short lifetime of less than three time-steps (18-h) are removed.

(5) The area enclosed by the outermost closed contour (OCC) is taken as the TPV domain, and the average distance between OCC and the TPV center is the radius of the TPV.

(6) If a low-pressure system is generated outside the TP (the boundary is shown in Fig. 1a), it has to travel inside the TP more than three time steps during its lifetime.

(7) There are a lot of low pressure systems produced due to the high resolution and fine contour-tracing (compared with Lin 2015), some of them are too weak to be defined as TPVs. However, most of them are not associated with precipitation. In addition, the difference in TPVs between various reanalysis datasets may be caused by the difference in TPVs between various reanalysis datasets may be caused by the difference of horizontal resolution, the dynamics and the parameterizations implemented in the numeric weather prediction model used and the assimilated observation to produce the reanalysis, instead of by the nature of TPVs. Hence, to provide a robust database for TPVs, the TPVs should be similar in the total number between different reanalysis datasets. The tuning of thresholds is based on the associated precipitation and comparison with the TPV yearbook (Li et al. 2001–2009; Institute of Plateau Meteorology, 2010–2018). The details are described in the support information (see Text.S1 and Fig. S3–S7). A TPV should satisfy the criterion that its radii during its lifespan are larger than the specified threshold for at least three time steps (Table 1). This criterion is kind of subjective and is set to exclude too small and too weak systems. A similar approach was used by Murakami (2014) to analyze tropical cyclones (TCs) based on reanalysis datasets. In his study, different parameters are specified for different reanalysis products for the purpose to obtain a similar number of TCs.

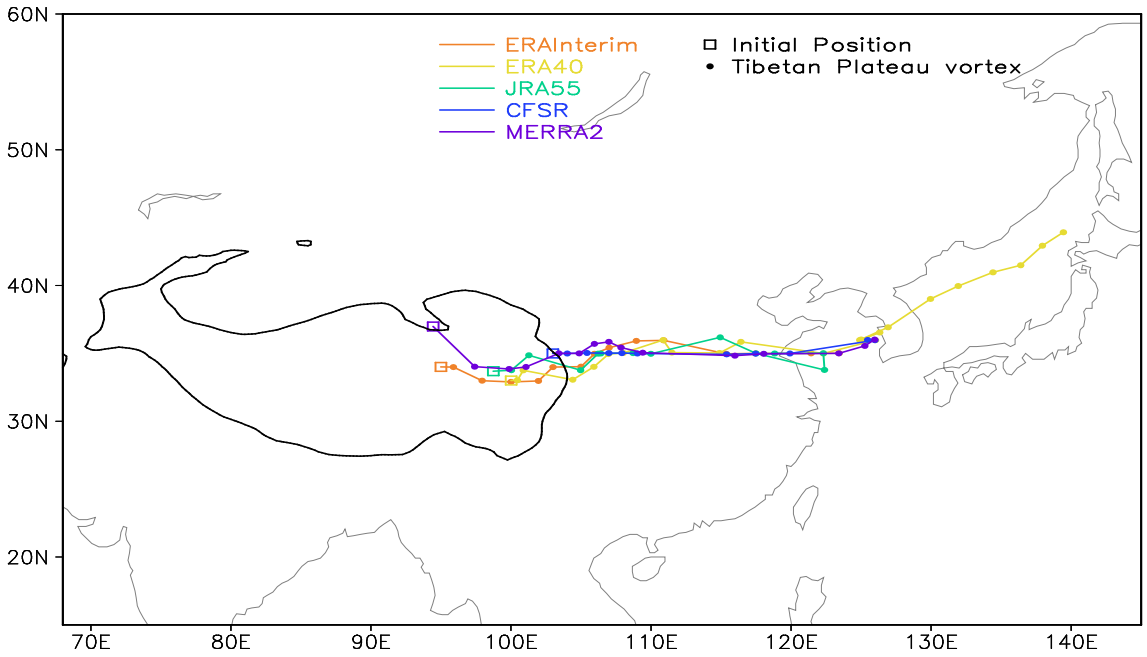

Fig. 1 The TPV case in June 1998. The square indicates the genesis position of the TPV. The thick line shows the 3000 m isohypse, representing the outline of the TP

The tracking of TPV is based on an inertial displacement algorithm proposed by WS06: (1) the displacement of a TPV should be less than 1000 km in 6 h; and its latitudinal component should be less than 400 km because the TPVs mainly move along the westerlies; (2) a TPV is supposed to move along its last movement which is defined as first guess position (FGP), and the initial position is taken as FGP when it's firstly detected, the nearest candidate low to FGP is chosen (WS06; Lin 2015). The detection and tracing of TPVs has some similar features as the cut-off lows, which is the low pressure systems embedded in the westerlies (e.g. Nieto et al. 2008 and references therein). The database of TPVs produced by this study has been posted on Science Data Bank (https://www.sciencedb.cn/dataSet/handle/556), which is a data source available freely to the public.

2.3 Typical cases

The tracks of two typical TPVs from different reanalysis products are shown in Figs. 1 and 2.

Averaged precipitation over the Yangtze River basin during June–August of 1998 was 670 mm, much higher than the multi-year mean during the same period. The cloud systems associated with the rainstorms in the Yangtze River basin in 1998 were triggered by perturbations originating in the TP and then moving eastward (Tao and Ding 1981; National Meteorological Center and National Satellite Meteorological Center 1998). Figure 1 shows a typical TPV observed in June 1998, which later triggered the heavy rainstorm and skyrocketing water levels in the middle reaches of the Yangtze River and lakes along the river. This TPV originated in the northeastern Tibetan Plateau, and dissipated near the Korean Peninsula after moving eastward out of the plateau. The TPV lasted the longest in the ERA40 and dissipated until it reached north of the Sea of Japan. All the five reanalysis products can well describe the complete process of the TPV activity, although there exist slight differences in its genesis position and life span.

Figure 2 presents an eastward moving TPV in June 2008. In all the reanalysis products, the TPVs originate in the western TP, and then move eastward along the shear line. These TPVs moved out of the TP in western Sichuan. Similar to the previous case, this TPV moved eastward along the Yangtze River and dissipated in eastern China. It triggered heavy rainstorms and floods in Sichuan, Hubei, and Anhui (Li et al. 2011). The complete lifespan of the TPV and associated circulations are similar in all the reanalysis products, and the TPV positions in the reanalysis products are close at individual analysis time.

The above two typical TPV cases demonstrate that the TPVs derived from different reanalysis products have similar tracks. More statistics of TPVs from various reanalysis products will be given later.

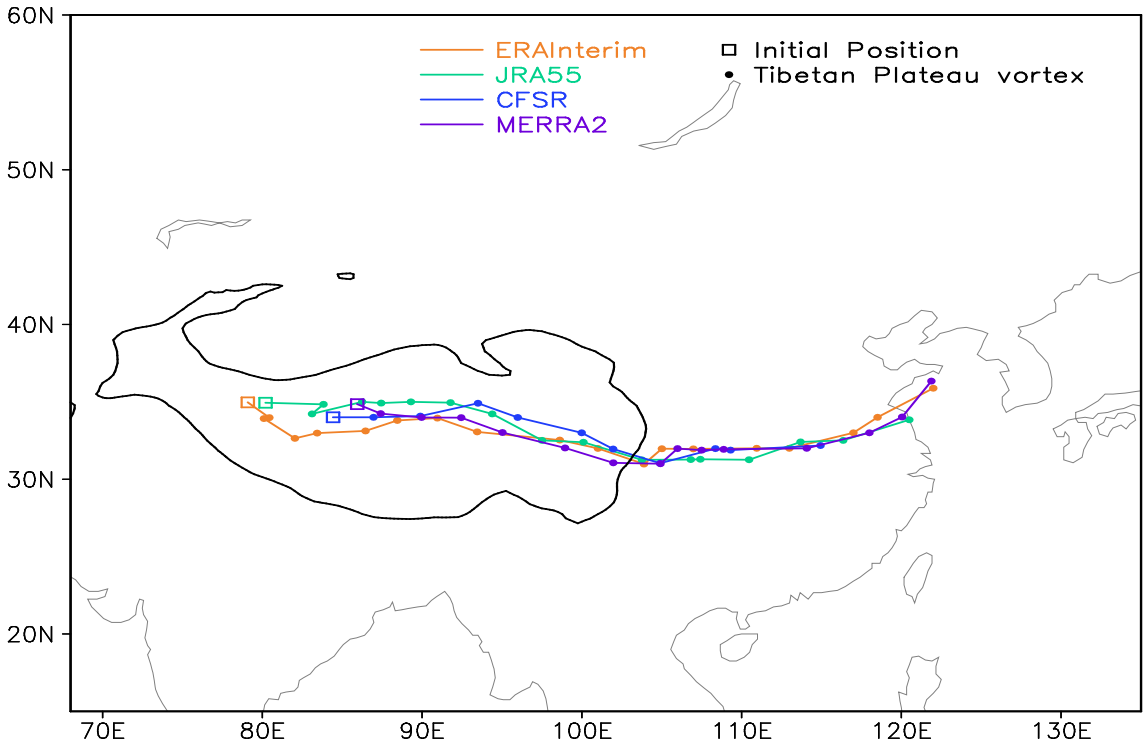

Fig. 2 Same as Fig. 1 but for the TPV in June 2008

3 Spatiotemporal variations of the TPV

3.1 Spatial distribution

The generation and dissipation positions of a TPV refer to the starting position and the last position it can be detected, respectively. The geographic distributions of the TPV generation and dissipation positions are important features of the TPV climatology.

Figure 3 denotes that TPVs are generated in two zonal genesis regions, i.e., over 78–95° E along 34° N (northern part) and over 84–90° E along 30° N (southern part) in the central TP (30–35° N, 75–98° E). The northern part extends eastward from Bango to northern Naqu, roughly located along the Karakoram—Qiangtang Plateau with

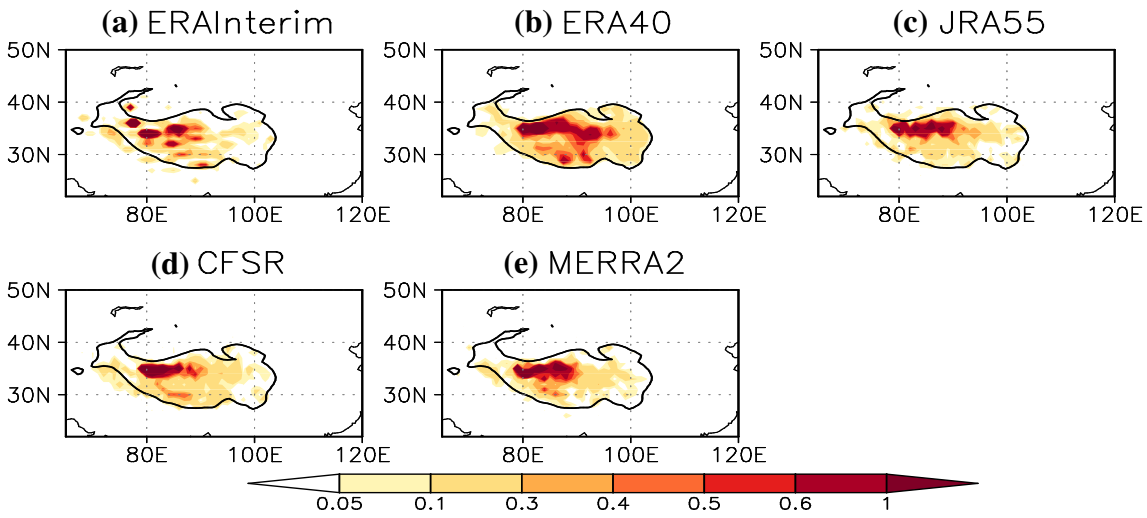

Fig. 3 Annual mean amount of TPVs generated within a box of 1° lon × 1° lat

the average elevation above 5500 m. The southern belt roughly coincides with the Gangdese Mountains—Nyainqentanglha Mountains. The northern belt is consistent with the TPV origin proposed in previous studies. Wang et al. (2009) named it a northeastern Naqu-Gaize-Shenzha belt. In the present study, the southern belt is detected due to higher resolution data and finer contour intervals implemented. The southern belt is part of the Naqu belt of high TPV genesis in previous studies. The relatively low-elevation area between the Gangdise Mountains and the Qiangtang Plateau corresponds to the low frequency of TPV genesis region. The close relationship between the distribution of TPV genesis and topography indicates that the TPVs are highly correlated with the topography-induced convergence and strong local heating (Feng et al. 2014). Compared to the manually identified TPVs in yearbooks (Li et al. 2002–2009; Institute of Plateau Meteorology, 2010–2018), the genesis position of TPVs based on reanalysis products and objective identification method is located further west. The genesis difference has been revealed by previous studies (Feng et al. 2014; Lin 2015; Curio et al. 2019). Curio et al. (2018) compared TPVs identified via manual and objective tracking, and found that there are two main reasons for the difference:

(1) it may be because the manual identification used the radiosonde network data with no observations to the west of 90 °E. The statistics of manually identified TPVs (Qian et al. 1984) shows that the number of TPVs in the western TP in 1979 is much larger than that in previous statistical results, which is attributed to the fact that more soundings were obtained in 1979 during the Atmospheric Science Experiment in the Tibetan Plateau;

(2) the other reason is that some TPVs are identified at the right beginning of their formation in the western TP, whereas they are manually identified as TPVs only when they deepened and moved to the east.

In the present study, the TPV genesis areas derived from high-resolution reanalysis datasets like MERRA2 (Fig. 3d) and CFSR (Fig. 3e) are more concentrated in the western TP compared to that derived from coarse-resolution datasets like JRA55 (Fig. 3c). More TPVs generated at the western TP in the present study compared to that of Lin (2015), despite the fact that ERAI is used in both studies. This is because the tracing contour intervals of geopotential height filed [in step (2) described in Sect. 2.3] in the present study are finer than that in Lin (2015), which makes it possible to detect TPVs when they are still weak and located in the western TP.

Most of the TPVs follow the westerlies to propagate eastward and dissipate in the central and eastern TP (Fig. 4) over (90–100° E, 32–36° N), which is a valley enclosed by Nyainqentanglha Mountain to the south side, Bayankala Mountain to the north and Tanggula Mountain to the west. The area near (80° E, 35° N) is another region where most stationary TPVs dissipate.

Some TPVs can move out of the TP and most of these TPVs reach the Sichuan Basin and the middle and lower reaches of the Yangtze River, as shown in the two cases described in the present study (described in Sect. 2.3, Figs. 1 and 2). Several previous studies also described the similar situation (Luo 1992; Feng et al. 2014; Yu et al. 2014; Lin 2015; Li et al. 2017, 2018a, b; Curio et al. 2019). Compared with the broad region where the eastward moving TPVs dissipate, those TPVs that move southward or northward usually dissipate in a small area adjacent to the TP. The

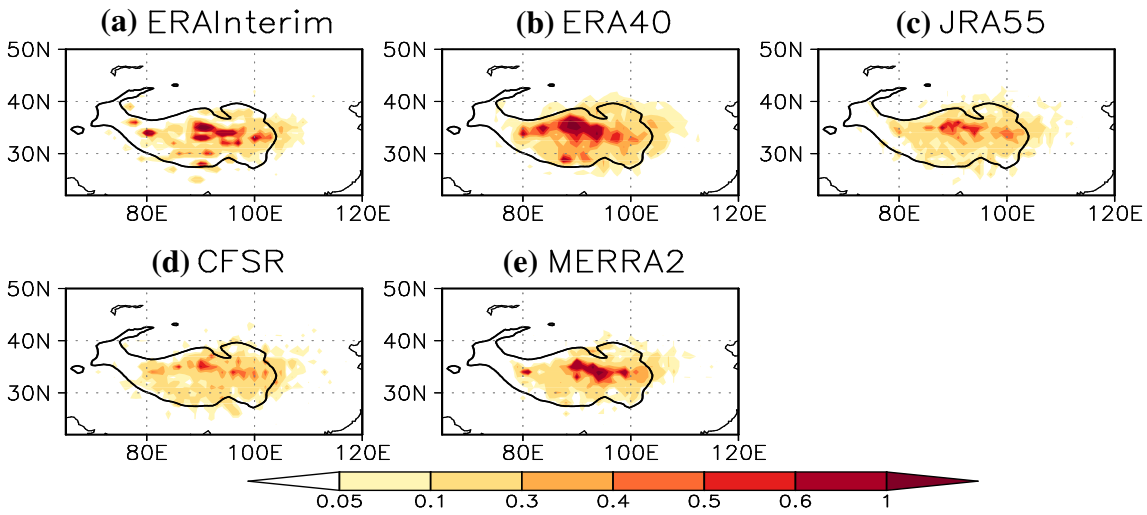

Fig. 4 Same as Fig. 3, but for the dissipation of TPVs

TPV tracks will be discussed in Sect. 4 of the present paper. In summary, most of the TPVs dissipate near their genesis area in the western TP, or over the low-elevation area in the downstream and lee sides of high mountains.

3.2 Diurnal variation

All the five reanalysis products indicate that the highest frequency of TPV formation occurs in the late afternoon (12:00 GMT, about 20:00 local time) and the smallest frequency occurs in the early morning (00:00 GMT), as shown in Fig. 5. More TPVs generate in the nighttime (12:00 and 08:00 GMT) than in the daytime (00:00 GMT and 06:00 GMT). The highest frequency of TPV dissipation occurs in 00:00 GMT. The diurnal variation of the frequency of TPV dissipation is less obvious than that of TPV genesis in all the reanalysis products. The diurnal variations of the TPV genesis and dissipation are consistent with the diurnal variations of precipitation and latent heat flux over the TP (Guo et al. 2014), but they are not consistent with the diurnal variation of sensible heat flux which is stronger in daytime, as revealed by Li et al. (2014a, b) and Feng et al. (2014). This fact implies that the atmospheric heating by latent heat release associated with precipitation is probably the primary factor that controls the TPV formation and development (Li et al. 2014b). Numerical experiments of Dell'osso and Chen (1986) and Shen et al. (1986a, b) yielded the same results.

3.3 Monthly variation

Figure 6 shows that the monthly variation of the occurrence frequency of TPV exhibits a unimodal feature. The peak appears in June and July, accounting for 20% of the annual total TPVs. The lowest frequency occurs in December and January with the TPVs less than 1% of the annual total. The second highest frequency occurs in May and August. In ERA40 and JRA55, the frequency in May is slightly higher than that in August (the difference is less than 2%); in CFSR and MERRA2, the frequency in August is higher than that in May (the difference is larger than 3%). When considering the distribution of standard deviation, it is obvious that the distributions in May and August are quite similar. Several previous studies also showed similar monthly variation features (Lin 2015; Feng et al. 2014; Wang et al. 2009), including the relatively high and low values in May and August. For example, based on ERAI, the frequency in May is higher than that in August (Lin 2015); in CFSR, however, the opposite is true (Feng et al. 2014). The feature that the frequency decreases rapidly after August (Feng et al. 2014) can also be found in the present study, which is obvious in JRA55 and MERRA2, while the decrease in ERAI and ERA40 is less dramatic. The TPV occurrence frequency is the highest in the summer, followed by that in the spring, and it is the smallest in the winter. This is a common feature reflected in all the reanalysis products. The warm season in the TP (May–September) is also the active period of the TPV, when about 80% of the TPVs appear during this period. The difference of active season for TPVs between reanalysis datasets ERAI and CFSR is also reported by Feng et al. (2014) and Curio et al. (2019).

3.4 Interannual variation

As shown in Fig. 7, the annual mean number of TPVs averaged over the five reanalysis products is approximately 63.5, with low numbers ranging within 37–50 and large numbers ranging within 74–87 among the reanalysis data. The standard deviations (STDs) are between 7.2 and 11.1. The smallest STD is from ERAI, indicating the ERAI yields the smallest interannual variability. The largest STD is from CFSR,

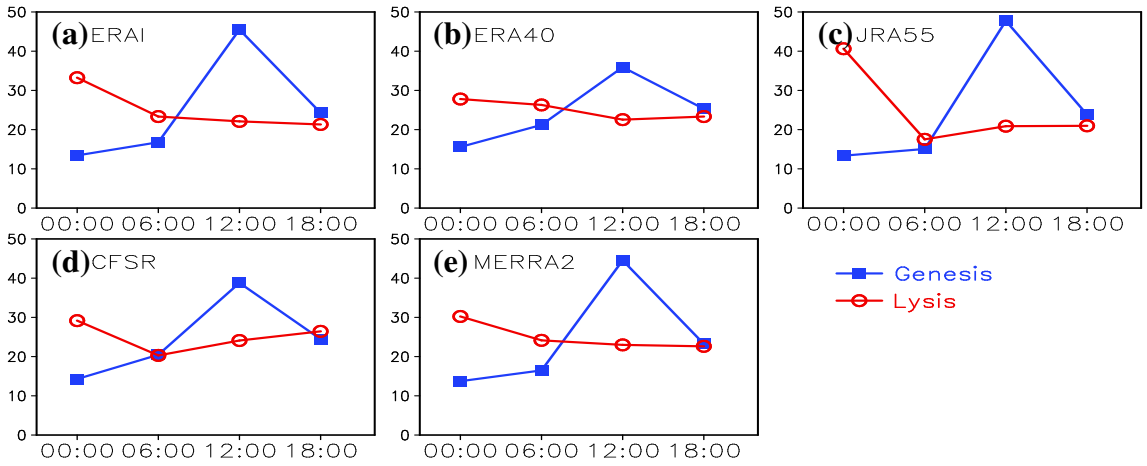

Fig. 5 Diurnal variation of the relative frequency (%) of TPVs; the X-axis is shown in UTC, it is 8 h ahead of the local time, thus 00:00 and 06:00 are daytimes, and 12:00 and 18:00 are nighttimes

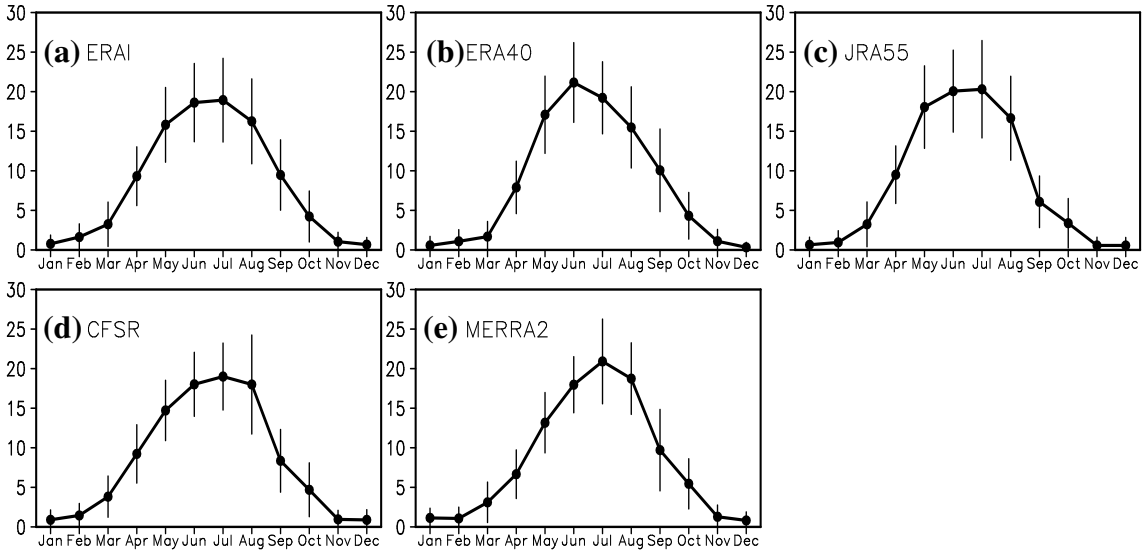

Fig. 6 Monthly variation of the relative TPV frequency (%). The vertical lines represent the standard deviations

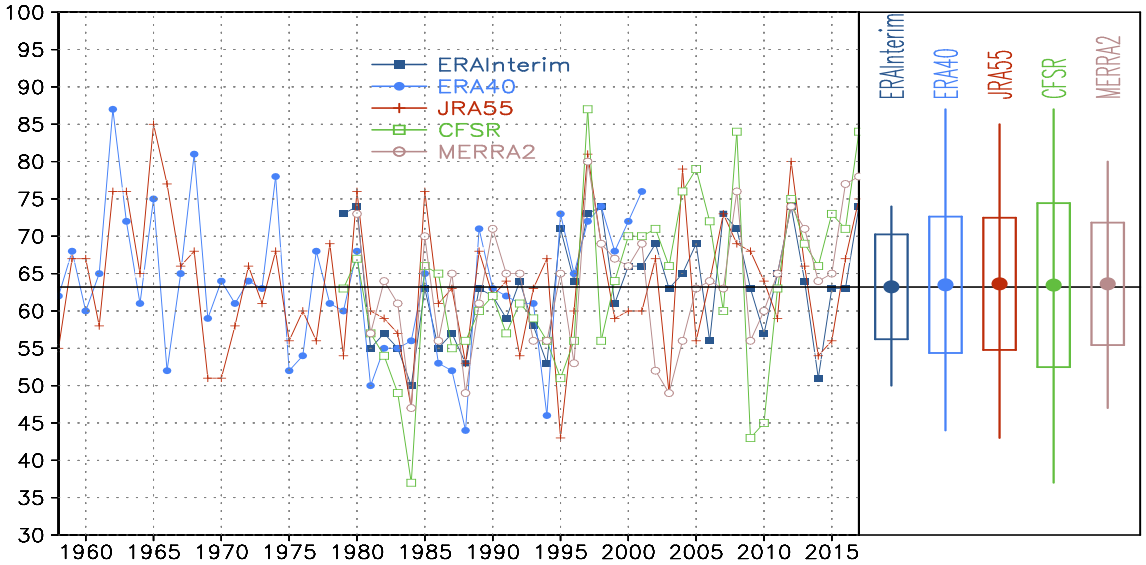

Fig. 7 Interannual variability of the annual number of TPVs derived from each reanalysis dataset. The solid lines show the annual numbers in the left graphic. The dots in the boxes plot denote the average numbers, the boxes denote the standard deviations, and the lines show the maximum and minimum values in the right graphic

which shows the largest interannual variability. The annual mean number of TPVs is slightly lower than that manually identified by Wang et al. (2009) (68/year), but higher than that (53/year) identified from ERAI by Lin (2015). The TPV number of 32 in the summer is similar to that found by Li et al. (2014a, b, c). The annual number of TPVs identified is dependent on the threshold like the TPV intensity, lifespan and genesis position, etc. Although the interannual variability of TPV is consistent in all the datasets (as shown in Fig. 7), the changing trend is different during different periods and between different datasets. This is why the changing trend of the TPV occurrence frequency is different in some previous studies (like Lin 2015 and Li et al. 2014a, b, c).

High correlations are found between the annual numbers of TPVs derived from various datasets (shown in the upper right corner of Table 2). The correlation coefficients between annual numbers of TPVs derived from the datasets used in the present study all are significant at the 0.01 level except that between the numbers from CFSR and ERA40, which is 0.453 and significant at the 0.05 level (23a in total, 1979–2001). Note that only those periods when data are available in both datasets are considered. The correlations

Table 2 Correlation coefficients between the number of TPVs and TPV frequencies derived from various datasets

	ERAI	ERA40	JRA55	CFSR	MERRA2
ERAI	–	**0.787**	**0.44**	**0.53**	**0.572**
ERA40	**0.848**	–	**0.367**	0.453	**0.645**
JRA55	**0.621**	**0.459**	–	**0.466**	**0.498**
CFSR	**0.71**	**0.551**	**0.644**	–	**0.58**
MERRA2	**0.682**	**0.646**	**0.655**	**0.736**	–

Bold indicates significance at 0.01 level. The number of TPVs and TPV frequency are calculated as: while a TPV maintained for *N* time steps, it would be counted as 1 single TPV, but the TPV frequency is counted as *N*

between TPV occurrence frequencies (total time steps of TPVs) derived from these individual datasets all are significant at 0.01 level (shown in the bottom left corner of Table 2). The high correlations between multiple datasets indicate that it is practical to investigate the climatological feature of TPV based on reanalysis products. The comparison of the TPV activities and tracks between multiple datasets are given in Sect. 5.

4 Characteristic parameters of the TPV

4.1 Lifespan

The lifespan of a TPV refers to the period from its genesis to its disappearance. Although a TPV in each specific time step is conducted at an instantaneous time, here it is considered to be lasting for 6-h. In other words, a single time analysis reveals the vortex condition during a 6-h period. Thereby, the lifespan is regarded as $H = 6 \times N$, where N is the number of times of a TPV appearing in analysis products. The lifespan of the TPV ranges from the shortest (the minimum threshold) of 18 h to the longest of almost 15 days. The lifespan of most TPVs in the reanalysis products is within 30–36 h except that in the JRA55, in which most of TPVs have a life span of one day (shown in Fig. 8a). Among all the reanalysis products, the TPVs with a lifespan shorter than two days occur most frequently and account for more than 60% of all TPVs, while those with a lifespan longer than 5 days only occur occasionally and account for less than 5% of all TPVs. Further analysis indicates that most of the TPVs (about 95%) with a lifespan longer than five days are also

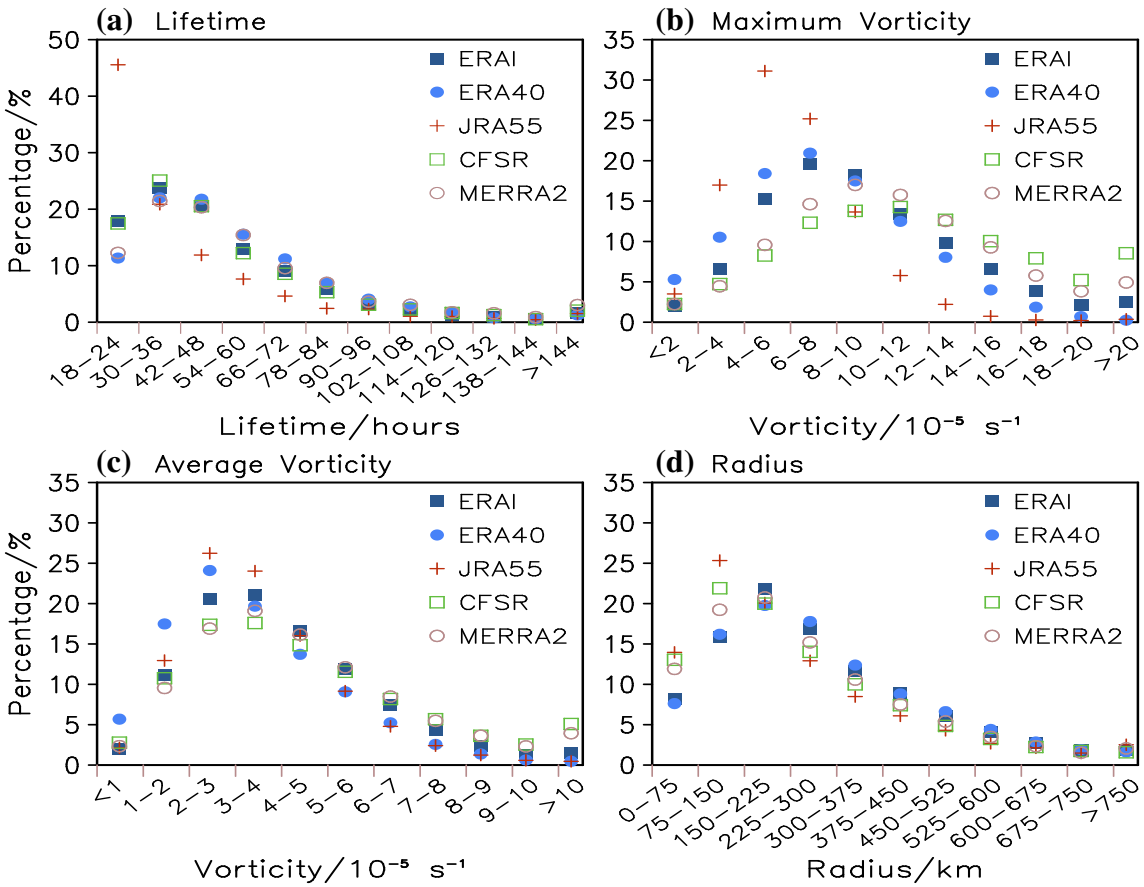

Fig. 8 Frequency distributions of TPV parameters: **a** lifespan; **b** maximum vorticity; **c** mean vorticity; **d** spatial scale

the TPVs that can move out of the TP. The average lifespan of TPVs in JRA55 is the shortest, which is probably attributed to the fact that the resolution of JRA55 is the coarsest among all the five datasets. The life span of TPVs in the five datasets follows the order of MERRA2 > CFSR > ERAI > ERA40 > JRA55, which implies that the lifespan of TPVs in a given reanalysis product might be related to the resolution of the reanalysis: the TPVs with longer lifespan are detected from datasets with higher resolution.

4.2 Intensity

The probability distribution function (PDF) of TPV intensity, which is measured by the maximum vorticity within the area of the TPV, is displayed in Fig. 8b. The PDFs from the five datasets all exhibit a unimodal pattern. The largest probability of intensity is $4 \sim 6 \times 10^{-5}$ s^{-1} in JRA55, and $6 \sim 8 \times 10^{-5}$ s^{-1} in ERAI and ERA40. However, the peak of PDFs in ERAI is larger than that in ERA40, indicating that the TPV intensity in ERAI is stronger than that in ERA40 with a small account of TPVs whose intensity is above 20×10^{-5} s^{-1}. The probability of TPVs with the intensity larger than 20×10^{-5} s^{-1} is most frequent in CFSR (about 10%), followed by that in MERRA2 (5%) and ERAI (3%), and is the least in JRA55 and ERA40 (less than 1%).

Figure 8c presents the PDF of the TPV intensity measured by the mean vorticity averaged over the area of the TPV. The pattern is similar to that in Fig. 8b. It displays a skewed distribution with the mean vorticity values concentrated around $2 \sim 4 \times 10^{-5}$ s^{-1}. Less than 2% of the TPVs from ERA40, ERAI and JRA55 can reach the intensity of 10×10^{-5} s^{-1}. However, the TPV intensity is relatively high in CFSR and MERRA2, with about 5% of the TPVs than can reach the intensity of 10×10^{-5} s^{-1}.

4.3 Spatial scale

The radii of TPVs from these datasets all show a unimodal distribution pattern with the peak values ranging within 100 ~ 250 km (shown in Fig. 8d). More than 75% of the TPVs from the five datasets have a radius ranging within 100 ~ 500 km, which is consistent with previous studies of the TPV scale, i.e., the TPV is a mesoscale synoptic system (Lhasa Research Group on Qinghai-Xizang Plateau Meteorology 1981; Luo 1992; Lin 2015; Hunt et al. 2018). Furthermore, ERAI and ERA40 have fewer small-scale TPVs but more large-scale TPVs (larger than 225 km). Small and large TPVs both are fewer in JRA55. The situations in CFSR and MERRA2 are between the ERAI/ERA40 and JRA55.

4.4 Tracks of TPVs moving out of the plateau

TPVs moving out of the TP tend to induce more precipitation downstream than over the TP. However, only a limited number of TPVs can move out of the TP. Depending on reanalysis products, the TPVs moving out of the TP account for about 11.5 ~ 14.3% of all TPVs (as shown in Table3). This ratio is similar to that revealed by Wang et al. (2009), Yu et al. (2007) and Lin (2015). The TPVs are classified into three types based on their disappearing positions, i.e., eastward moving, northeastward moving, and southward moving.

(1) The eastward moving TPVs are the most common type, which account for 7.1 ~ 7.9% of all TPVs and 60% of those moving out of the TP. As shown in Fig. 9a, these TPVs may originate anywhere over the TP and dissipate over a broad region from Sichuan Basin to the middle and lower reaches of the Yangtze River valley after moving out of the TP. This eastward moving path actually includes the southeastward path proposed by Yu et al. (2014). Only a few parts of TPVs move out of the TP following the southeastward path and these TPVs usually dissipate in Yunnan-Guizhou Plateau.
(2) The northeastward moving TPVs accounts for 2.1–3.9% of all TPVs and 19–30% of those moving out of the TP. Most of the TPVs originate to the north of 30° N and dissipate over the Loess Plateau and southern Xinjiang after moving out of the TP, as shown in Fig. 9b.
(3) The TPVs moving southward are the least, which account for 1.3 ~ 2.8% of all TPVs and 10 ~ 19% of those moving out of the TP. This path has never been found before, and it might be due to the fact that the analyzed radiosonde network is mainly located in China. To inspect the reliability of this moving path, we have examined each individual TPV that is identified as moving out of the TP following this path. As

Table 3 Annual mean numbers of TPVs moving out of the TP following various paths, and the relative ratios to all TPVs (in brackets) for the five reanalysis datasets

	All moving off	Eastward path	Northeastward path	Southward path
ERAI	8.4 (12.9%)	4.9 (7.6%)	2.4 (3.8%)	1.1 (1.5%)
ERA40	7.3 (11.5%)	4.5 (7.1%)	1.4 (2.2%)	1.4 (2.3%)
JRA55	8 (12.6%)	5 (7.8%)	2.2 (3.5%)	0.8 (1.3%)
CFSR	8.8 (13.9%)	4.4 (6.9%)	2.8 (4.4%)	1.6 (2.5%)
MERRA2	9.1 (14.3%)	4.8 (7.6%)	2.5 (3.9%)	1.8 (2.8%)

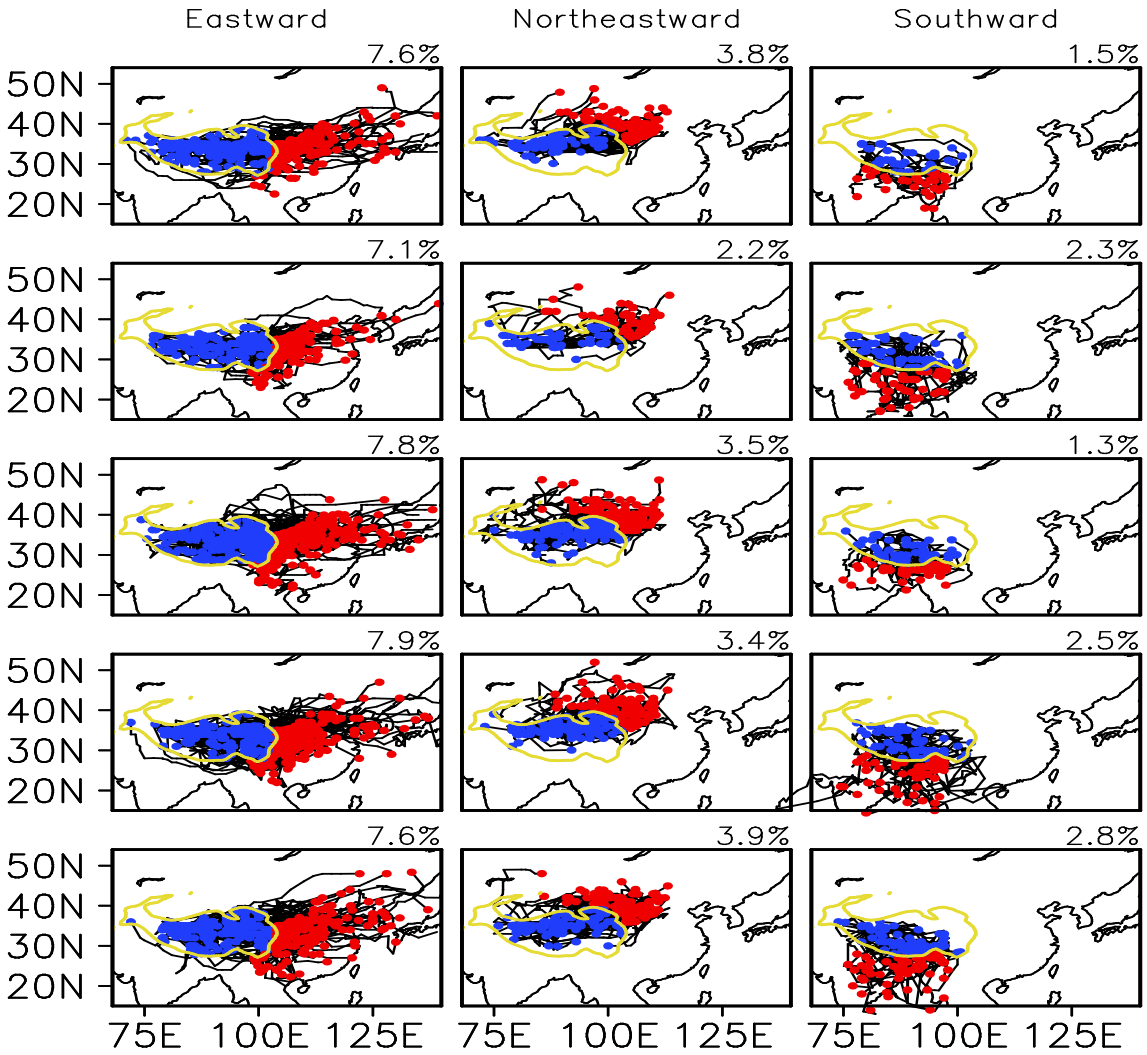

Fig. 9 Paths of TPVs moving out of the TP. The number on the upper right corner of each panel is the percentage of TPVs following the specific path, the blue dots denote the genesis positions of TPVs, the red dots indicate the positions where TPVs disappear, the thin black lines show the TPV paths, the thick yellow line indicates elevation above 3000 m. From top to bottoms are results from ERAI, ERA40, JRA55, CFSR, MERRA2, respectively; from left to right shows the westward path, the northeastward path, and the southward path, respectively

shown in Fig. 9c, it is found that these TPVs mostly originate in the southwestern TP and dissipate in the northern India Peninsula and Bay of Bengal. Fig. S10 shows the composited large-scale circulation, which has a pattern different to that corresponding to the other two paths (shown in Figs. S8 and S9). It indicates that TPVs move southward out of the TP when the Iranian high-pressure system at 500 hPa intensifies and extends eastward to the western TP. These TPVs moved out of the TP under the steering flow of northwesterly over western TP. This special path may imply that the TPVs can affect the northern Indian Peninsula, an aspect that has not been revealed in earlier studies which may be due to that only the eastward TPVs are identified as the moving-off cases, e.g. Curio et al. (2019) and Li et al. (2020).

5 Differences between various reanalysis products

In order to further analyze the consistency of TPVs in various reanalysis datasets, the TPVs from each dataset are compared with those from other datasets. If the distance between a given TPV in one dataset and the TPV at the same time in another dataset is less than 500 km, then the TPV position is regarded as matching with the reanalysis dataset. If more than 50% positions or four time steps of a given TPV in one

dataset match with that in another dataset, then the TPV path is regarded as matching with the dataset.

5.1 Difference in the TPV paths

Table 4 lists the matching rates of TPVs between various reanalysis products. Each number in Table 4 represents the matching rate between TPV paths for the dataset shown in the corresponding row and column. For example, in total there are 2466 TPVs in ERAI and 1501 out of 2466 TPVs can match with those from ERA40, and thus the matching rate is $1501/2466 \times 100\% = 60.9\%$.

Table 4 shows that the matching rates between various datasets all are above 50% except that with JRA55. Higher matching rates indicate that the reanalysis products are consistent with each other with respect to the TPVs. Therefore, it is practical to study TPVs based on reanalysis products as proposed by Lin et al. (2013), Feng et al. (2014), Lin (2015) and Curio et al. (2019). The matches between multiple reanalysis products suggest that ERAI may be the best dataset for TPV study, followed by the MERRA2.

The critical factor that affects the matching rate is the lifespan of the TPV. Figure 10 shows that TPVs with longer lifespan often correspond to a larger matching rate. Those TPVs that last longer than 4 days show 60–80% of consistency between various datasets, while those last less than 2 days show only 25–50% of consistency. This is partly because TPVs with longer lifespan are also TPVs with stronger intensity (Feng et al. 2014), and stronger TPVs may have higher possibility to be matched in various datasets. TPVs that move out of the TP have a much longer lifespan (Li et al. 2014b, 2018a, b; Yu et al. 2014, 2016; Feng et al. 2014).

Table 4 Matching rates (%) of TPV track between various datasets

	ERAI	ERA40	JRA55	CFSR	MERRA2
ERAI	–	*60.9*	47.7	59.7	**62.4**
ERA40	**57.9**	–	38.7	50.6	*52.1*
JRA55	**63.1**	55.2	–	57.6	*60.2*
CFSR	*59.9*	53.7	42.3	–	**60.6**
MERRA2	**59.3**	50.7	42.1	*55.9*	–

Each number is the matching rate between datasets in its corresponding row and column. The maximum (second largest) value in each row is in bold (italic)

5.2 Differences in the position of TPV

Table 5 lists the matching rates of TPV positions derived from multiple reanalysis datasets. Compared with the matching rates of TPV paths, the matching rates of TPV positions are relatively low. Further examination reveals that the position matching rates for TPVs that match in their paths are

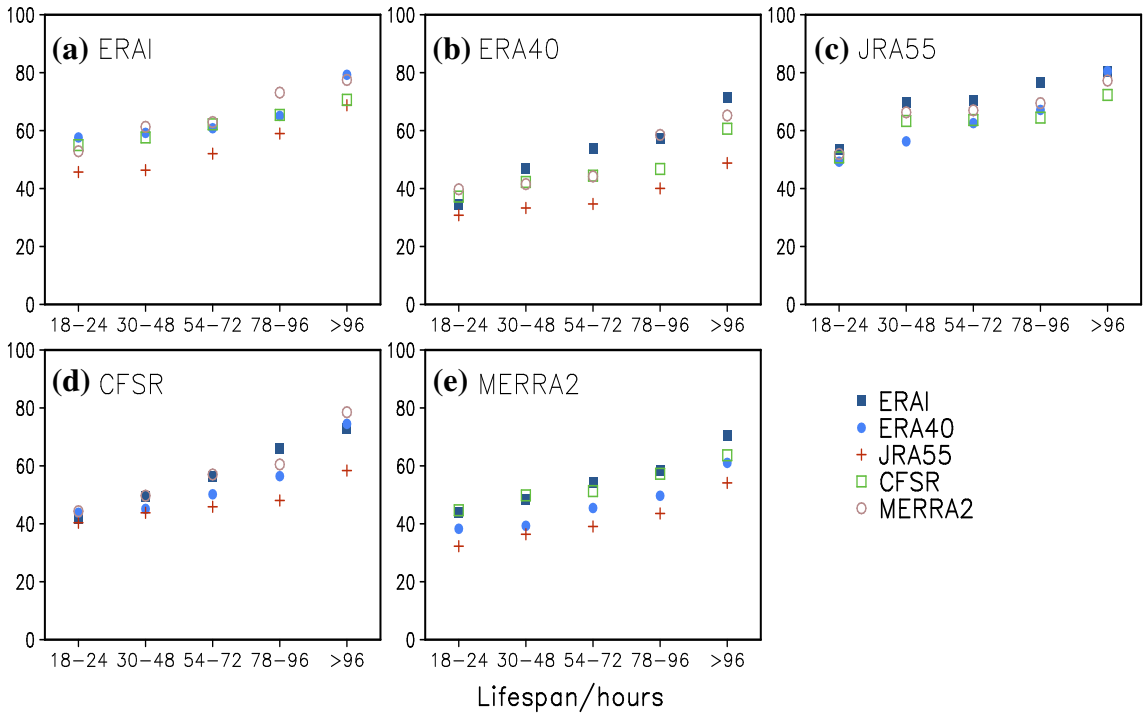

Fig. 10 Distributions of the matching rate (%) between various reanalysis datasets for TPVs of various lifespans derived from: **a** ERA-Interim; **b** ERA40; **c** JRA55; **d** CFSR; **e** MERRA2

Table 5 Matching rates (%) of TPV positions

	ERAI	ERA40	JRA55	CFSR	MERRA2
ERAI	–	*57.3*	48.6	57.2	**60.8**
ERA40	**53.6**	–	39.8	46.1	*50.1*
JRA55	**61.6**	54.4	–	56.2	*60.4*
CFSR	*55.2*	49.5	42.9	–	**56.7**
MERRA2	**53.5**	47	41.8	*51.1*	–

Each number is the matching rate between the datasets in the corresponding row and column. The maximum (second largest) value in each row is in bold (italic)

much higher than that unmatched. It is not unexpected that the ERAI is the best with respect to the matching rate. The MERRA2 ranks the second.

Following the increase in the TPV intensity, the TPVs become more consistent in different datasets (as shown in Fig. 11). Generally, stronger TPVs are often accompanied with longer lifespan, more precipitation and higher possibility to move out of the TP, and thus can have more significant impact. The high consistency of TPVs in various datasets suggests that the results of the present study can be a helpful reference for the study of TPV activities. Based on the matching rates of TPV detection and TPV paths, the usability of the five reanalysis datasets for tracking TPVs can be ranked as ERAI > MERRA2 > CFSR > ERA40 > JRA55.

6 Discussions

Table 6 lists the results of previous studies on the activity of TPVs. It presents a wide variance between results of the manual tracking and the objective tracking, which is largely attributed to difference for the identification of weak and small-size TPVs. The four major causes for the difference can be summarized as follows: the sparse observatory network over the TP, the subjectivity of manual identification or the parameters used in objective tracking, the difference in tracking method and variables used, and the performance of the reanalysis datasets (Curio et al. 2018). The common features of TPVs found in all results are: (1) the TPVs active months is the warm season, i.e., May–September; (2) more TPVs over the western TP can be detected from the reanalysis datasets than from the weather charts, and this is true no matter whether objective or manual detection method is used; (3) the moving off TPVs only account for a small part of total TPVs.

It seems that the identification based on relative vorticity tends to get more TPVs than that based on geopotential height. It might be attributed to two reasons: one is that a TPV can be detected in its earlier genesis stage via relative vorticity when it appears without a low pressure center; the other is that some cyclonic systems such as troughs and fronts might be mistakenly identified as TPVs.

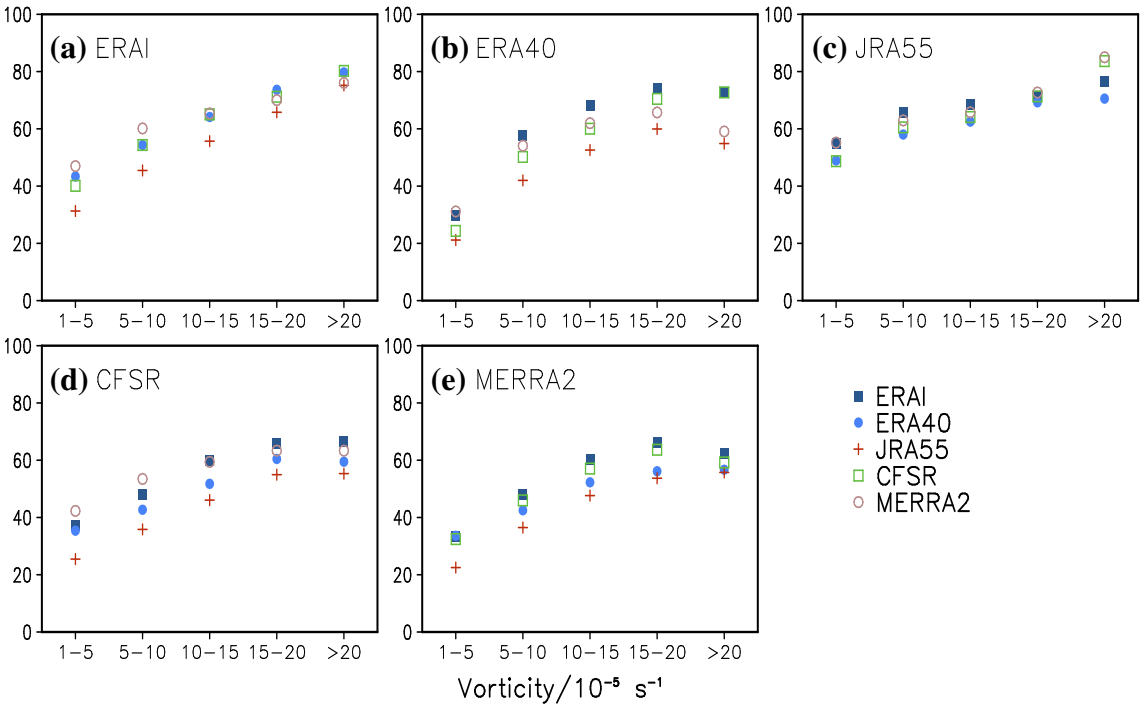

Fig. 11 Distribution of the matching rate (%) between various reanalysis datasets for TPVs with various maximum vorticity derived from: **a** ERA-Interim; **b** ERA40; **c** JRA55; **d** CFSR; **e** MERRA2

Table 6 Annual mean TPVs numbers in previous studies

Main reference	Method	Data source	Variable used	Minimum lifespan	Minimum Intensity	Minimum size	Yearly mean (Seasons)	Mean amount (ratio) of moving off	Period
Wang et al. (2009)	Manual	Weather charts	Z & W	–	–	–	68 (May–Sep)	6.8 (10%)	1980–2004
Li et al. (2014a)	Manual	NCEP/NCAR	Z	–	–	–	32 (Jun–Aug)	1.3 (4%)	1980–2010
Feng et al. (2014)	Auto	CFSR	ζ	6-h	$\zeta > 0$	$L \geq 2°$	103 (Apr-Oct)	8.7 (8.5%)	2000–2009
Lin (2015)	Auto	ERA-Interim	Z	18-h	$\zeta > 0$	$A \geq 10^4$ km^2	53	6.7 (13%)	1979–2013
TPV yearbook	Manual	Weather charts	Z & W	–	–	–	45	9.7 (21%)	2001–2016
Curio et al. (2019)	Auto	ERA-Interim	ζ	24-h	$\zeta \geq 2$	$L \geq 400$ km	154	31 (20%)	1979–2015
–	Auto	CFSR	ζ	24-h	$\zeta \geq 2$	$L \geq 400$ km	269	53 (20%)	1979–2015
Present study	Auto	ERA-Interim	Z	18-h	$\zeta \geq 1$	$R \geq 145$ km	63.5	8.4 (12.9%)	1979–2017
–	Auto	ERA-40	Z	18-h	$\zeta \geq 1$	$R \geq 140$ km	63.5	7.3 (11.5%)	1958–2001
–	Auto	JRA55	Z	18-h	$\zeta \geq 1$	$R \geq 60$ km	63.5	8 (12.6%)	1958–2017
–	Auto	CFSR	Z	18-h	$\zeta \geq 1$	$R \geq 170$ km	63.5	8.8 (13.9%)	1979–2017
–	Auto	MERRA2	Z	18-h	$\zeta \geq 1$	$R \geq 155$ km	63.5	9.1 (14.3%)	1980–2017

ζ is relative vorticity at 500 hPa, with a unit of 10^{-5} s^{-1}; Z is geopotential height at 500 hPa; W is horizontal wind at 500 hPa; L is the horizontal dimension of TPV; A is the area of TPV; R is radius of TPV. In last 5 rows, the "minimum size" and the "minimum intensity" column means the TPVs should satisfy the both conditions for at least 3 time steps in lifetime span. The "minimum size" of Curio et al (2019) is operated by the spectral filtering to remove total wave-numbers larger than 100 (smaller than 400 km)

In general, objective identification and tracking of TPVs based on reanalysis and other model-based datasets can be the direction of future TPV studies. It is automatic and reproducible compared to manual tracking, especially when huge amounts of data need to be processed. As pointed out by Curio et al. (2019), the high-resolution global climate model can represent the TPV climatology. Therefore, identification of TPVs can be used to reveal its development mechanism in the long-term modeling instead of modeling a single case, and can be used to assess the future of TPVs with the models' projection (e.g. CMIP6).

7 Summary

Five widely used reanalysis datasets, i.e., ERAI, ERA40, JRA55, CFSR and MERRA2, are used in the present study to investigate the climatological features of the TPVs. The TPVs and related parameters are posted on the website to provide helpful information for the studies of the TPVs. The main conclusions are as follows.

(1) High spatiotemporal consistency is found between multiple reanalysis datasets, including the spatial distribution of the TPV genesis and dissipation, the diurnal cycle of the TPV activity, the seasonal and interannual variability of the TPV. The matching rates of the TPV paths and positions are high between different datasets. The highest matching rates are found for ERAI, followed by those for MERRA2. The matching rates are the lowest for JRA55 due to its coarse resolution.

(2) The annual mean number of TPV genesis is about 63.5, which mainly form at the high-elevation area above 5500 m and dissipate in valleys and the lee side of the eastern TP slope, where the elevation is relatively low. Most of the TPVs occur in the warm season (May–September). More TPVs form in the nighttime than in the daytime, while the opposite is true for their dissipation.

(3) Probability distribution functions of the TPV lifespan, intensity and spatial scale are obtained, which indicate that TPVs from high-resolution datasets usually have longer lifespan, stronger relative vorticity, and larger spatial scale.

(4) Less than 15% of the TPVs can move out of the TP, and they follow the eastward, northeastward, and southward paths. The eastward path is the primary path for TPVs to move out of the TP, and the southward path is first revealed in the present study.

The climatology of TPVs had been investigated through variant data source, i.e. the weather charts and reanalysis datasets. The comparable difference between reanalysis datasets brings some different performance of TPVs due to the data sources (Curio et al. 2018, 2019; Li et al. 2020). However, even the yearbooks of the TPVs are not fully reliable, due to the lack of observation data and the subjectivity

of artificial identification. This study provides the basic climatological characteristics of the TPVs through multiple reanalysis datasets, and provides a database for other studies. The high consistency of the TPV's characteristics produced by variant reanalysis datasets shows the robustness of the present studies to avoid the uncertainties of individual data source. Therefore, the objective identification method has potentiality to assess the future changes of TPVs from model-based datasets (Curio et al. 2019), the results obtained in this study can afford a baseline for the performance assessment and the parameter adjustment. A feasible way to obtain the best dataset of the TPVs is to synthesize the results derived from various methods and different data sources, just like the efforts on the tropical cyclone (Knapp et al. 2010). Our work might be an imperfect but important step to achieve that goal.

Acknowledgements This research is sponsored by the Strategic Priority Research Program of Chinese Academy of Sciences (Grant No.XDA2006010104), the National Natural Science Foundation of China (Grants No.41775075, No.91637105), and the National Special Project for Commonweal Industry in China (Grant No.GYHY201406001). We thank the information provided by Science Data Bank (https://www.sciencedb.cn). The Grid Analysis and Display System Software (GrADS) is used to analyze and display data.

References

Bao XH, Zhang FQ (2013) Evaluation of NCEP-CFSR, NCEP-NCAR, ERA-Interim, and ERA-40 reanalysis datasets against independent sounding observations over the Tibetan Plateau. J Climate 26:206–214. https://doi.org/10.1175/JCLI-D-12-00056.1

Cavall SM, Hakim GJ (2013) Physical mechanisms of tropopause polar vortex intensity change. J Atmos Sci 70:3359–3373. https://doi.org/10.1175/JAS-D-13-088.1

Curio J, Chen YR, Schiemann R, Turner AG, Wong KC, Hodges K, Li YQ (2018) Comparison of a manual and an automated tracking method for Tibetan plateau vortices. Adv Atmos Sci 35:965–980. https://doi.org/10.1007/s00376-018-7278-4

Curio J, Schiemann R, Hodges KI, Turner AG (2019) Climatology of Tibetan Plateau vortices in reanalysis data and a high-resolution global climate model. J Climate 32:1933–1950. https://doi.org/10.1175/JCLI-D-18-0021.1

Dee DP et al (2011) The ERA-Interim reanalysis: configuration and performance of the data assimilation system. Q J Meteor Soc 137A:553–597. https://doi.org/10.1002/qj.828

Dell'osso L, Chen SJ (1986) Numerical experiments on the genesis of vortices over the Qinghai-Xizang Plateau. Tellus 38A:236–250

Feng XY, Liu CH, Rasmussen R (2014) A 10-yeasr climatology of Tibetan Plateau Vortices with NCEP Climate Forecast System Reanalysis. J Appl Meteor Climatol 53:34–46. https://doi.org/10.1175/JAMC-D-13-014.1

Gelaro R et al (2017) The modern-era retrospective analysis for research and applications, version 2 (MERRA-2). J Clim 30:5419. https://doi.org/10.1175/JCLI-D-16-0758.1

Guo JP et al (2014) Diurnal variation and the influential factors of precipitation from surface and satellite measurements in Tibet. Int J Clim 34(9):2940–2956. https://doi.org/10.1002/joc.3886

Hanley J, Caballero R (2012) Objective identification and tracking of multicentre cyclones in the ERA-Interim reanalysis dataset. Q J R Meteor Soc 138:612–625. https://doi.org/10.1002/qj.948

Hu L, Deng DF, Xu XD, Zhao P (2017) The regional differences of Tibetan convective systems in boreal summer. J Geophy Res Atmos 122:7289–7299. https://doi.org/10.1002/2017JD026681

Hunt KMR, Curio J, Turner AG, Schiemann R (2018) Subtropical westerly jet influence on occurrence of western disturbances and Tibetan Plateau vortices. Geophy Res Lett. https://doi.org/10.1029/2018GL077734

Immerzeel W, van Beek L, Bierkens MF (2010) Climate change will affect the Asian water towers. Science 328(5984):13825984. https://doi.org/10.1126/science.1183188

Institute of Plateau Meteorology, published during 2011–2018. Year book of Tibetan Plateau vortex and shear line (2010–2016). Science Press, Beijing.

Knapp KR, Kruk MC, Levinson DH, Diamond HJ, Neumann CJ (2010) The international best track archive for climate stewardship (IBTrACS): unifying tropical cyclone data. Bull Am Meteor Soc 91(3):363–376. https://doi.org/10.1175/2009BAMS2755.1

Kobayashi S et al (2015) The JRA-55 reanalysis: general specifications and basic characteristics. J Meteor Soc Jpn 93:5–48. https://doi.org/10.2151/jmsj.2015-001

Lhasa Research Group on Qinghai-Xizang Plateau Meteorology (1981) A study of 500-mb vortexes and Shearlines over the Qinghai-Xizang plateau in the warm season. Science Press, Beijing, p 122 **(in Chinese)**

Li GP, Zhao FH, Huang CH, Niu JL (2014a) Analysis of 30-year climatology of the Tibetan Plateau vortex in summer with NCEP reanalysis data. Chin J Atmos Sci 38(4):756–769. https://doi.org/10.3878/j.issn.1006.9895.2013.13235 **(in Chinese)**

Li L, Zhang RH, Wen M (2011) Diagnostic analysis of the evolution mechanism for a vortex over the Tibetan Plateau in June 2008. Adv Atmos Sci 25(4):797–808. https://doi.org/10.1007/s00376-010-0027-y

Li L, Zhang RH, Wen M (2014b) Diurnal variation in the occurrence frequency of the Tibetan Plateau vortices. Meteor Atmos Phys 125:135–144. https://doi.org/10.1007/s00703-014-0325-5

Li L, Zhang RH, Wen M, Liu LK (2014c) Effect of the atmospheric heat source on the development and eastward movement of the Tibetan Plateau vortices. Tellus A 66:24451. https://doi.org/10.3402/tellusa.v66.24451

Li L, Zhang RH, Wen M, Lv JM (2018a) Effect of the atmospheric quasi-biweekly oscillation on the vortices moving off the Tibetan Plateau. Clim Dyn 50(3–4):1193–1207. https://doi.org/10.1007/s00382-017-3672-3

Li L, Zhang RH, Wen M (2017) Genesis of southwest vortices and its relation to Tibetan Plateau Vortices: genesis of SWVs and its Relation to TPVs. Q J R Meteor Soc 143:2556–2566. https://doi.org/10.1002/qj.3106

Li L, Zhang RH, Wu PL (2020) Evaluation of NCEP-FNL and ERA-Interim data sets in detecting Tibetan Plateau vortices in May–August of 2000–2015. Earth Space Sci. https://doi.org/10.1029/2019EA000907

Li XF, Fowler HJ, Forsythe N, Blenkinsop S, Pritchard D (2018b) The Karakoram/Western Tibetan vortex: seasonal and year-to-year variability. Clim Dyn. https://doi.org/10.1007/s00382-018-4118-2

Lin HB, You QL, Zhang YQ, Jiao Y, Fraedrich K (2016) Impact of large-scale circulation on the water vapour balance of the Tibetan Plateau in summer. Int J Climatol 36:4213–4221. https://doi.org/10.1002/joc.4626

Lin ZQ (2015) Analysis of Tibetan Plateau vortex activities using ERA-Interim data for the period 1979–2013. J Meteor Res 29(5):720–374. https://doi.org/10.1007/s13351-015-4273-x

Luo SW (1992) A study of some kinds of weather systems over and around the Qinghai-Xizang Plateau. Meteorology Press, Beijing, p 205 **(in Chinese)**

Li YQ, and Coauthors, published during 2009–2010. Year book of Tibetan Plateau vortex and shear line (1998–2009). Science Press, Beijing.

Murakami H (2014) Tropical cyclones in reanalysis data sets. Geophys Res Lett 41:2133–2141. https://doi.org/10.1002/2014GL059519

National Meteorological Center and National Satellite Meteorological Center (1998) China Catastrophic Flood in 1998 and Weather Forecasts. Meteorology Press, Beijing, p 382 **(in Chinese)**

Neu U et al (2013) IMILAST: a community effort to intercompare extratropical cyclone detection and tracking algorithms. Bull Am Meteor Soc 94:529–547. https://doi.org/10.1175/BAMS-D-11-00154.1

Nieto R, Sprenger M, Wernli H, Trigo RM, Gimeno L (2008) Identification and climatology of cut-off lows near the tropopause. Ann NY Acad Sci 1146:256–290. https://doi.org/10.1175/10.1196/annals.1446.016

Qian ZA, Shan FM, Lv JN, Cai YX, Chen YC (1984) Statistics of Qinghai-Xizang Plateau vortices for the summer of 1979 and discussions of the climatological factors for the vortex genesis. Collected Works of QXPMEX(II), Science Press, Beijing, pp 182ijingtics hinese)

Qiu J (2008) The third pole. Nature 454(7203):393–396. https://doi.org/10.1038/454393a

Saha S et al (2010) The NCEP climate forecast system reanalysis. Bull Am Meteor Soc 91:1015. https://doi.org/10.1175/2010BAMS3001.1

Shen RJ, Reiter ER, Bresch JF (1986a) Numerical simulation of the development of vortices over the Qinghai-Xizang Plateau. Meteor Atmos Phys 35:70–95

Shen RJ, Reiter ER, Bresch JF (1986b) Some aspects of the effects of sensible heating on the development of summer weather systems over the Qinghai-Xizang Plateau. J Atmos Sci 43:2241–2260

Tao SY, Ding YH (1981) Observational evidence of the influence of the Qinghai-Xizang (Tibet) Plateau on the occurrence of heavy rain and severe convective storms in China. Bull Am Meteor Soc 62:23

Uppala SM et al (2005) The ERA-40 reanalysis. Q J R Meteor Soc 131:2961–3012. https://doi.org/10.1256/qj.04.176

Wang B (1987) The development mechanism for Tibetan Plateau warm vortices. J Atmos Sci 44:2978–2994

Wang X, Li YQ, Yu SH, Jiang XW (2009) Statistical study on the Plateau low vortex activities. Plateau Meteor 28:64–71 **(in Chinese)**

Wernli H, Schwierz C (2006) Surface cyclones in the ERA-40 dataset, part I: novel identification method and global climatology. J Atmos Sci 63:2486–2507. https://doi.org/10.1175/JAS3766.1

Xu XD, Lu CG, Shi XH, Gao ST (2008a) World water tower: an atmospheric perspective. Geophy Res Lett. https://doi.org/10.1029/2008GL035867

Xu XD et al (2008b) A new integrated observational system over the Tibetan Plateau. Bull Am Meteor Soc 89(10):1492–1496. https://doi.org/10.1175/2008BAMS2557.1

Yao TD et al (2012) Different glacier status with atmospheric circulations in Tibetan Plateau and surrounding. Nat Clim Change 2:633–667. https://doi.org/10.1038/NCLIMATE1580

Ye DZ, Gao YX (1979) Meteorology of Qinghai-Xizang (Tibetan) Plateau. Science Press, Beijing, pp 45–53 **(in Chinese)**

Ye DZ (1981) Some characteristics of the summer circulation over the Qinghai-Xizang (Tibet) plateau and its neighborhood. Bull Am Meteor Soc 62:14–19

You QL, Min JZ, Zhang W, Pepin N, Kang SC (2015) Comparison of multiple datasets with gridded precipitation observations over the Tibetan Plateau. Clim Dyn 45:791–806. https://doi.org/10.1007/s00382-014-2310-6

Yu SH, Gao WL, Peng J, Xiao YH (2014) Observational facts of sustained departure plateau vortexes. J Meteor Res 28:296–307. https://doi.org/10.1007/s13351-014-3023-9

Yu SH, Gao WL, Xiao D, Peng J (2016) Observational facts regarding the joint activities of the southwest vortex and plateau vortex after its departure from the Tibetan Plateau. Adv Atmos Sci 33(1):34–46. https://doi.org/10.1007/s00376-015-5039-1

Zhang PF, Li GP, Fu XH, Liu YM, Li LF (2014) Clustering of Tibetan Plateau vortices by 10–30 day intraseasonal oscillation. Mon Wea Rev 142:290–300. https://doi.org/10.1175/MWR-D-13-00137.1

Zhang SL, Tao SY, Zhang QY, Zhang XL (2001) Meteorological and hydrological characteristics of severe flooding in China during the summer of 1998. Q J Appl Meteor 12(4):442–457 **(in Chinese)**